https://doi.org/10.5194/egusphere-2024-2641
Preprint. Discussion started: 18 September 2024

Estimating the variability of NO_x emissions from Wuhan with TROPOMI NO_2 data during 2018 to 2023

Qianqian Zhang[1], K. Folkert Boersma[2,3], Chiel van der Laan[4], Alba Mols[2], Bin Zhao[5,6], Shengyue Li[5,6], Yuepeng Pan[7,8]

[1]National Satellite Meteorological Center, Key Laboratory of Radiometric Calibration and Validation for Environmental Satellites, Innovation Center for Fengyun Meteorological Satellite (FYSIC), China Meteorology Administration, Beijing 100081, China
[2]Wageningen University, Environmental Science Group, Wageningen, the Netherlands
[3]Royal Netherlands Meteorological Institute, De Bilt, the Netherlands
[4]Eindhoven University of Technology, Eindhoven, the Netherlands
[5]State Key Joint Laboratory of Environmental Simulation and Pollution Control, School of Environment, Tsinghua University, Beijing 100084, China
[6]State Environmental Protection Key Laboratory of Sources and Control of Air Pollution Complex, Beijing 100084, China.
[7]Key Laboratory of Atmospheric Environment and Extreme Meteorology, Chinese Academy of Sciences, Beijing 100029, China
[8]College of Earth and Planetary Sciences, University of Chinese Academy of Sciences, Beijing 100049, China

Correspondence to: Qianqian Zhang, zhangqq@cma.gov.cn

Abstract. Accurate NO_x emission estimates are required to better understand air pollution, investigate the effectiveness of emission restrictions, and develop effective emission control strategies. This study investigates and demonstrates the ability of the superposition column model in combination with TROPOMI tropospheric NO_2 column data to estimate city-scale NO_x emissions and lifetimes and their variabilities. Using the recently improved TROPOMI tropospheric NO_2 column product (v2.4–2.6), we derive daily NO_x emissions and lifetimes over the city of Wuhan for 335 clear sky days between May 2018 and December 2023. We find a slight weekend reduction in NO_x emission with a weekend-to-weekday ratio of 0.95 and a small seasonal variation of NO_x emissions over Wuhan with a summer-to-winter emission ratio of 0.87. We calculate a steady decline of NO_x emissions from 2019 to 2023, and the emission in 2023 is ~15% below the 2019 level, indicating the success of the emission control strategy. The estimated NO_x lifetimes range from 0.8 h (summer) to 5.3 h (winter), with an average of 2.6 h. Meanwhile, our method shows ~30% lower NO_x lifetimes for fast wind (> 7 m s^{-1}) speed. The superposition model method results in ~10% lower estimation of NO_x emissions when the wind direction is from distinct upwind NO_2 hotspots compared to other wind directions, indicating the need to improve the approach for cities that are not relatively isolated pollution hotspots. The results of this work nevertheless confirm the strength of the superposition column model in estimating urban NO_x emissions with reasonable accuracy.

https://doi.org/10.5194/egusphere-2024-2641
Preprint. Discussion started: 18 September 2024

1 Introduction

Nitrogen oxides ($NO_x \equiv NO_2 + NO$) are key atmospheric components affecting the formation of particulate matter and ozone (Goldberg et al., 2019; Zhang et al., 2021). They are emitted into the atmosphere mainly from the combustion of fossil fuels, which takes place primarily in urban areas, to heat and provide electricity to homes and businesses and to run cars and factories. Cities are responsible for more than 70% of global NO_x emissions, and this proportion increases with the process of global urbanization and industrialization (Park et al., 2021; Stavrakou et al., 2020; Baklanov et al., 2016). Thus, accurate NO_x emission inventories for cities are required for monitoring the effectiveness of reducing air pollution and for global and regional chemical models to reproduce the complicated urban air pollution (Beirle et al., 2011). Bottom-up city NO_x emission inventories are quite uncertain in the emission factors (Lu et al., 2015) and during the down-scaling from national or regional emissions to city level (Butler et al., 2008; Lamsal et al., 2011).

NO_2 has long been detected by remote sensing instruments with high quality because of its strong spectral features within the ultraviolet/visible spectrum, and various satellite instruments have been providing tropospheric NO_2 column measurements for near-surface NO_x emissions estimation for tens of years (Burrows et al., 1999; Bovensmann et al., 1999; Levelt et al., 2006; Veefkind et al., 2012). Limited by the early, coarse spatial resolution, researchers computed the global or regional long-term mean NO_x emissions with satellite observations and chemical transport models (CTMs) (Martin, 2003; Lamsal et al., 2011; Kharol et al., 2015). With the improving capabilities of later satellite sensors, more researchers started to estimate NO_x emissions on higher spatial and temporal resolutions but still depended on CTMs (Ding et al., 2017; Visser et al., 2019; Xing et al., 2022). However, there are barriers to access and employment of CTMs, and there is a substantial computational burden when our target is a single city. Therefore, CTM-independent methods have been developed and applied to estimate NO_x emissions since the early 2010s (Beirle et al., 2011; De Foy et al., 2014; Kong et al., 2019; 2019; Lorente et al., 2019; Rey-Pommier et al., 2022).

Beirle et al. (2011) rotated the 2-dimensional NO_2 map surrounding a large point source (such as a megacity or a power plant, factory) toward the wind direction and integrated NO_2 columns perpendicular to the wind to obtain the so-called NO_2 line density along the wind direction. They developed an Empirical Modified Gaussian model (EMG) to estimate city NO_x emissions and chemical lifetime from the increase of NO_2 over the city and its decay downwind of the city. The model has been refined (Valin et al., 2013), validated (De Foy et al., 2014; 2015), applied (Lu et al., 2015; Lange et al., 2022; Goldberg et al., 2019) and extended (Liu et al., 2016; 2022). The EMG model has been applied to OMI NO_2 data to calculate NO_x emissions from cities, power plants, and factories across the globe and was shown to be accurate when wind speed is larger than 2 or 3 m s^{-1}. In addition, this model requires a relatively large study area and is limited to calculating the mean NO_x emissions averaged over a longer time period.

https://doi.org/10.5194/egusphere-2024-2641
Preprint. Discussion started: 18 September 2024

At present, the much improved spatial resolution and retrieval quality of the TROPOMI sensor makes it possible to track the NO_2 distribution and downwind plume over the city from a single satellite overpass. Based on a single TROPOMI overpass, Lorente et al. (2019) narrowed down the study area to the domain of one city and developed a superposition column model to fit the NO_2 line density for daily NO_x emissions on (sub-)city scale. Zhang et al. (2023) used this model to estimate the daily variation of NO_x emissions over Wuhan from September 2019 to August 2020. The superposition column model avoids the bias caused by the use of the average of the NO_2 product in the nonlinear system to calculate mean NO_x lifetimes and emissions (Valin et al., 2013).

In this study, we continue to focus on the city of Wuhan, extend our study period from May 2018 to December 2023, and estimate city NO_x emissions and lifetimes on a daily basis. Our purpose is, first, to demonstrate the ability of the superposition column model to provide information on city NO_x emissions and lifetimes on interannual, seasonal, and weekly variations influenced by changes in human activity; second, to investigate the model performance influenced by the meteorology (wind speed and directions). The rest of the paper is organized as follows: Section 2 introduces the data and methods we employ in this study. In Section 3, we compare our results with those of other studies, analyze the temporal variability of NO_x emissions and lifetimes over Wuhan, investigate the dependence of our estimations on the wind field, and discuss the uncertainties in this work. The conclusion remarks are presented in Section 4.

2 Data and Material

2.1 TROPOMI NO_2 tropospheric columns

On 13 October 2017, the Copernicus Sentinel-5 Precursor (S-5P) satellite was successfully launched into sun-synchronous orbit with the local overpass time at around 13:30. The TROPOspheric Monitoring Instrument (TROPOMI) is the only instrument on board S-5P, dedicated to air quality and climate monitoring. TROPOMI observes NO_2 at 405–465nm of the UV-visible spectral band with an unprecedented nadir spatial resolution of 3.5×5.5 km^2 (as of 6 August 2019) (Van Geffen et al., 2020; 2022). The small pixels and large swath width (approximately 2600 km) of TROPOMI allow the detection of localized point sources and downwind NO_2 plumes from cities on a daily basis (Beirle et al., 2019; Lorente et al., 2019).

This work uses the operational TROPOMI NO_2 version 2.4.0–2.6.0 algorithm from May 2018 to December 2023. The version 2.3.1 includes a different treatment of the surface albedo compared to the earlier versions, which led to a 10~15% increase of tropospheric NO_2 columns over polluted scenes (Van Geffen et al., 2022). There is a major change from version 2.3.1 to 2.4.0. In v2.4.0, a new TROPOMI surface albedo climatology (Directional Lambertian Equivalent Reflectivity, DLER) was implemented in the cloud fraction and cloud pressure retrievals and air-mass factor calculation (Eskes et al., 2023). The use of DLER results in a substantial increase of NO_2 columns in vegetated regions, and the higher resolution ($0.125° \times 0.125°$) of DLER better resolves the variability in the surface albedo (Keppens and Lambert, 2023). The v2.4.0 version made a complete mission reprocessing from 1 May 2018 to 22 July 2022 and then switched to the offline mode until

https://doi.org/10.5194/egusphere-2024-2641
Preprint. Discussion started: 18 September 2024

12 March 2023. The version 2.5.0 implemented a minor bug fix concerning the qa_value field over snow or ice-covered regions. The version 2.6.0 started on 16 November 2023, exactly the same as version 2.5.0.

The version 2.4.0–2.6.0 Level 2 tropospheric NO_2 products are reported to be biased between +33% (over cleaner areas) and –50% (over highly polluted areas) compared to the ground-based MAX-DOAS data from 29 stations, with the overall negative median bias being 28%. Amongst all the 29 ground stations, one is in north China, Xianghe. At Xianghe, the TROPOMI tropospheric NO_2 columns correlate ($R^2 = 0.88$) well with the MAX-DOAS data with a median low bias of ~20%, and the weekly averaged relative difference is within ±30% for most of the days (Keppens and Lambert, 2023). When we use the TROPOMI data in Wuhan, some low bias is expected, and we adjust a scale factor of 1.2 to (partly) correct the bias and screen each ground pixel for the quality assurance flag (qa_value) greater than 0.75.

2.2 Wind data and chemical parameters

Apart from the tropospheric NO_2 columns, wind field (wind direction and wind speed) and atmospheric chemical parameters are needed as forward model parameters to determine city NO_x emissions and lifetimes. We use the reanalysis of hourly wind data on pressure levels provided by the fifth-generation (ERA5) European Center for Medium-Range Weather Forecasts (ECMWF) (Hersbach et al., 2020). This dataset has a horizontal resolution of 0.25° × 0.25°, and we use the 3 levels mean meridional and zonal wind below 950hPa. The two hourly values immediately before and after the TROPOMI overpass timestamp are linearly interpolated.

The chemical parameters, including the hydroxyl radical (OH) concentration and atmospheric NO_x/NO_2 ratio, are obtained from version 12.3.2 GEOS-Chem chemical transport model simulations for lack of observations. The nested grid version of the GEOS-Chem model over East Asia (70°E−140°E, 15°N−55°N) operates full aerosol-oxidant simulation at 0.25° × 0.3125° spatial resolution with 47 vertical levels from ground to the top of the stratosphere (Zhang et al., 2015). The GEOS-Chem model is widely used and refined worldwide to simulate and evaluate the atmospheric aerosol and gas phase pollutants (https://geoschem.github.io/overview.html). It has been extensively found to be skillful in simulating the concentration and distribution of ozone, $PM_{2.5}$, and nitrate aerosols in China (Zhai et al., 2021; Geng et al., 2017; Lu et al., 2019; Li et al., 2019). Thus we can say that the GEOS-Chem model produces compelling predictions of chemical parameters of NO_x. This work uses the boundary layer mean OH concentration at 12:00−14:00 to predict prior values for the atmospheric NO_x chemical loss rate. As we stated in our previous work (Zhang et al., 2023), the GEOS-Chem simulated NO_x/NO_2 ratio varies less than 10% with seasons, so we use the fixed value of 1.26 in this work following Zhang et al. (2023).

2.3 Emission inventory

Initial guess of NO_x emission patterns and amounts are needed in this study, and we use the Air Benefit and Attainment and Cost Assessment System Emission Inventory (ABACAS-EI) (Zhao et al., 2013; Zhao et al., 2018; Zheng et al., 2019) to provide this information. The ABACAS-EI is available at 1km × 1km gridded resolution over China, and it is developed

https://doi.org/10.5194/egusphere-2024-2641
Preprint. Discussion started: 18 September 2024

based on activity rates and energy consumption levels with an estimated uncertainty of ±35% (Zhao et al., 2013; Li et al., 2024b). The Emission Database for Global Atmospheric Research (EDGAR) v6.1 of 2018 annual total is also used for comparison.

2.4 The superposition column model

Lorente et al. (2019) introduced this superposition column model to estimate city NO_x emissions and lifetimes based on a single TROPOMI overpass and determined daily NO_x emissions over Paris. Zhang et al. (2023) modified and used this model for the Chinese city of Wuhan in a more polluted background.

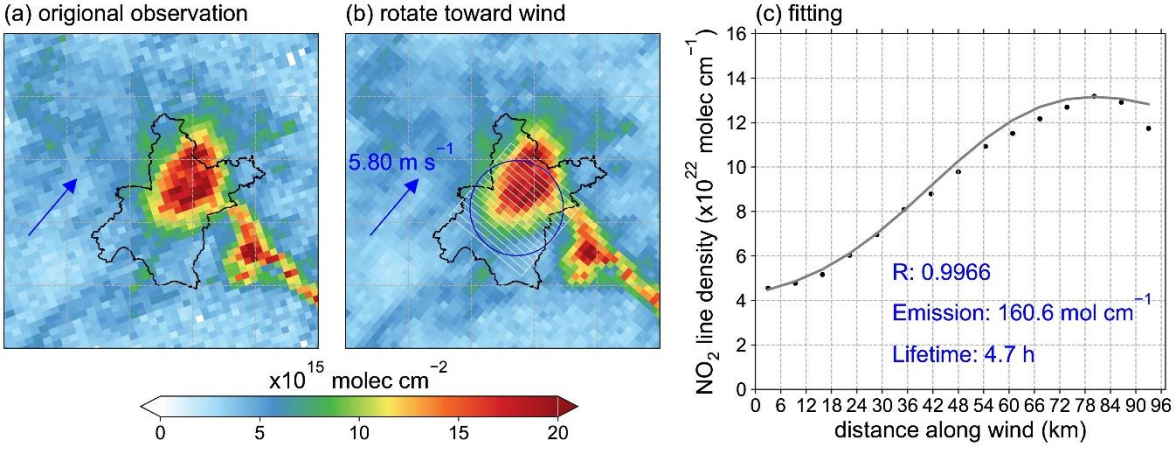

Figure 1: The analysis steps of the superposition column model. (a) The original TROPOMI NO_2 columns were on 4 March 2023. (b) NO_2 columns resampled at a grid map aligned with the wind direction. The blue circle inside denotes the study domain centered on Wuhan city center with a 45 km radius, and the white lines indicate the grid cells along with the wind direction. (c) Integrate the grid cells perpendicular to the wind direction to obtain the NO_2 line density and fit it with the superposition column model.

Using the day 4 March 2023 as an example, we demonstrate the analysis steps of the superposition column model (Fig. 1). We focus on the build-up of NO_2 columns over a 45 km radius of Wuhan city center (the blue circle in Fig. 1b). We construct a 15 × 15 grid map centered at the city center with each grid size of 0.05 °× 0.05 °(6km × 6km), and rotate the grid map toward the mean wind direction. The original TROPOMI observation (Figure 1a) is sampled into the rotated grid (Fig. 1b). The TROPOMI NO_2 columns in the 15 grid cells perpendicular to the wind direction are integrated to form the so-called NO_2 'line densities' (Beirle et al., 2011), resulting in 15 grid cells along the wind direction (Fig. 1c).

Then, the NO_2 line density is fitted with the superposition column model (Lorente et al., 2019; Zhang et al., 2023) which is based on a simple column model (Jacob, 1999). We solve each grid cell along the wind direction with a simple column model, NO_x builds up within the current cell and decays exponentially downwind of this cell.

https://doi.org/10.5194/egusphere-2024-2641
Preprint. Discussion started: 18 September 2024

$$N_i(x) = \frac{E_i}{k}\left(1 - e^{-kL/u}\right) \times e^{-k(x-x_i)/u} \times \frac{[NO_2]}{[NO_x]} \quad for\ x > x_i \ , \tag{1}$$

NO_x emissions from cell i (E_i, mol cm^{-1} s^{-1}) along the wind direction contribute ($N_i(x)$, mol cm^{-1}) to the overall line density through the build-up of NO_x within the current cell and exponential decay in the downwind cells (Eq. (1)). We assume a first-order loss of NO_2 reacted with OH in the atmosphere. In Eq. (1), k (s^{-1}) represents the loss rate of NO_x at the TROPOMI overpass time. k is determined by the atmospheric OH concentration ($[OH]$, molec cm^{-3}), the reaction rate constant k' between NO_2 and OH (here we use 2.6 × 10^{-11} cm^3 molec^{-1} s^{-1} from the GEOS-Chem model) and the NO_x/NO_2 ratio in the atmosphere: $k = \frac{k'[OH]}{[NO_x]/[NO_2]}$. L denotes the length of each grid cell, i.e. 6 × 10^5 cm, and u is the wind speed (cm s^{-1}). E_i has no contribution to the upwind cells (Eq. (2)).

$$N_i(x) = 0 \qquad for\ x \le x_i \ , \tag{2}$$

$$N(x) = \sum_{i=1}^{n} N_i(x) + b + \alpha x \ , \tag{3}$$

The contributions from all the 15 cells are stacked up to make the superposition column model, and with the contribution from the background NO_2 line densities ($b + \alpha x$) to obtain the overall $N(x)$ (Eq. (3)). The initial guess of the background value b is set as the NO_2 line density at the upend point $N(0)$.

The terms E_i, k, and α are fitted to the TROPOMI observed NO_2 line densities to determine $N(x)$. In the fitting procedure, we make some changes compared to Zhang et al. (2023). First, for the treatment of the initial guess of OH concentrations, considering the uncertainty in simulated OH concentrations, we use the monthly instead of daily mean noon time (12:00—14:00) boundary layer OH concentration as the initial guess for the daily inversion. We allow it to change between 0.3 to 2 times in lieu of the ±30% interval around the initial value; this range is chosen because most (more than 90%) of the simulated daily OH concentration falls in the 0.3 to 2 times the monthly mean value. Second, the combination of a least squares minimization of $N(x)$ to the TROPOMI observed line density $N_{TROPOMI}(x)$ and E_i to the ABACAS-EI NO_x emissions $E_{ABACAS,i}$ (Eq.(4)). We restrict the emissions to a gaussian shape and a scale factor is applied to the emission term. It is found to be ~0.1 for all the days that lead to the best fit of the NO_2 line densities. We make these modifications to the superposition column model because we are trying to dilute the dependence of fitted NO_x emissions on the OH concentrations, which are of significant uncertainty and have no solid observations (Zhang et al., 2021).

$$\text{func} = \left(\frac{N(x) - N_{TROPOMI}(x)}{N_{TROPOMI}(x)}\right)^2 + factor * \left(\frac{E_i - E_{ABACAS,i}}{E_{ABACAS,i}}\right)^2 \tag{4}$$

https://doi.org/10.5194/egusphere-2024-2641
Preprint. Discussion started: 18 September 2024

3 Results and discussion

3.1 Mapping Wuhan's NO_x emissions and comparison to other inventories

From May 2018 until December 2023, we collect 581 overpasses with clear skies over Wuhan. We remove the overpasses with inhomogeneous wind fields, which happen most frequently in winter. The inhomogeneous wind fields include the situations when the wind direction changes more than 45° within 2 hours before the satellite overpasses and the wind at zonal or meridional direction reverses at different pressure levels when the satellite overpasses. Multiple overpasses within one day are analysed separately to calculate NO_x emissions and then averaged for the daily mean emission level. We also exclude the days with estimated NO_x emissions beyond 0.5—1.5 times the ABACAS bottom-up emissions. The 0.5—1.5 times interval is chosen because it covers the uncertainty level of bottom-up NO_x emissions, the degree of seasonal and weekly variability, and the year-to-year change of NO_x emissions over Wuhan from 2018 to 2023. This standard is not applied when calculating NO_x emissions during the COVID-19 lockdown-influenced period (23 January 2020 to the end of April 2020).

Finally, we obtain a total of 335 days with valid NO_x emissions and lifetimes estimations. The number of valid days for each year and each season are summarized in Table 1. For the five years (2019—2023) with full-year measurement, the percentage of days with valid estimations is 14.0%—19.2%. Seasonally, we obtain the most valid days in autumn (defined as September to November), followed by summer (June to August). There are least valid days in winter (December to February) after spring (March to May) for the cloudy and polluted conditions in winter.

Table 1: Number of days with valid NO_x emissions and lifetime estimations for each year and each season.

By year	2018	2019	2020	2021	2022	2023
	26	64	59	65	70	51
By season[a]	Spring		Summer	Autumn		Winter
	70		71	119		50

a. The COVID-19 lockdown-influenced days (23 January to the end of April in 2020) are not considered when we count the valid days by season.

Zhang et al. (2023) used the superposition column model to calculate NO_x emissions over Wuhan for the period from September 2019 to August 2020. They calculated 11.5 kg s^{-1} (equivalent to about 250 mol s^{-1}) NO_x emissions over Wuhan (including the city center and the outskirts of Wuhan) from September to November 2019. We estimate 153.4±40.5 mol s^{-1} NO_x emissions over the central region of Wuhan for the same period, indicating ~60% of NO_x emissions are concentrated over the central area. Lange et al. (2022) applied the EMG function to calculate NO_x emissions over Wuhan from March 2018 to November 2020 (the COVID-19 lockdown-influenced period excluded) of 115.1±10.1 mol s^{-2}, and they used a much earlier TROPOMI data version 1.1.0—1.3.0 with larger low bias and they did not apply an ad hoc correction factor of 1.2 as

https://doi.org/10.5194/egusphere-2024-2641
Preprint. Discussion started: 18 September 2024

we do in this study. Zhang et al. (2023) estimated an average NO_x lifetime over Wuhan of 2.46 h, Lange et al. (2022) reported a 2.94±0.3 h. This study calculates a mean NO_x lifetime of 2.61 h, close to the previous studies.

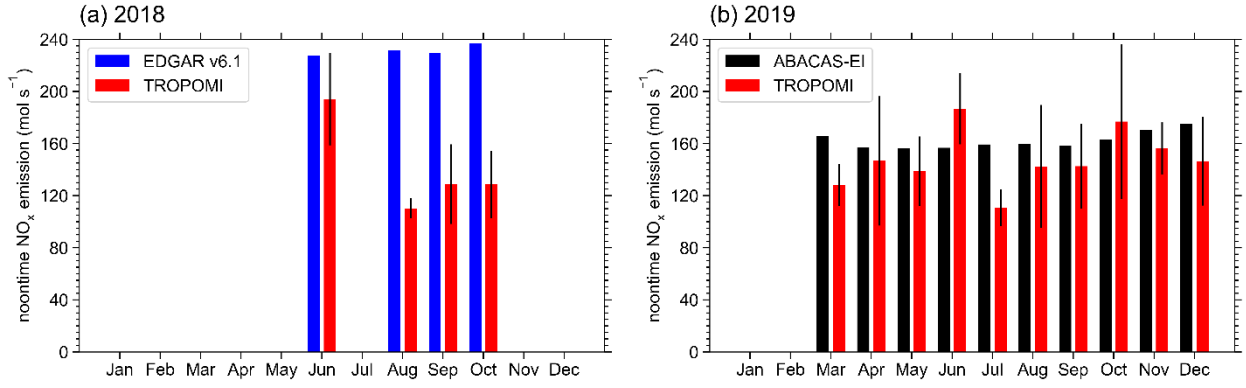

Figure 2: Monthly NO_x emissions estimated with the TROPOMI data (red), reported by EDGAR v6.1 (blue) and ABACAS-EI (black) for (a) 2018 and (b) 2019. The monthly mean is calculated only when three or more days are available. Thus, the comparisons are only possible for some months. The error bars on the TROPOMI estimations represent the standard deviation of the daily NO_x emissions in each month derived by the superposition column model.

We now compare the NO_x emissions over Wuhan estimated in this study with those from ABACAS-EI (for the year 2019) and EDGAR v6.1 (for the year 2018) in Figure 2. It needs to be pointed out that the annual total NO_x emissions are provided in the ABACAS-EI and EDGAR v6.1, and we convert them into monthly mean with the time factor in ABACAS-EI. Since the monthly mean NO_x emissions are calculated only when three or more days' NO_x emissions are available, we obtain only four months (June, August, September, and October) in 2018 and 10 months (March to December) in 2019. For 2018, we estimate monthly NO_x emissions over Wuhan of ~140.5 mol s^{-1}, while it is as high as ~230 mol s^{-1} estimated by EDGAR v6.1. Lange et al. (2022) also found a large discrepancy between satellite-derived and EDGAR bottom-up NO_x emissions over Wuhan and several other large cities. For 2019, the monthly NO_x emissions over Wuhan calculated by the superposition column model is ~4.7% lower than that from the ABACAS-EI, close to the difference reported by Zhang et al. (2023).

3.2 Temporal variability of NO_x emissions over Wuhan

Considering the atmospheric photochemical activity of NO_x, previous studies using the build-up of NO_2 pollution along the wind direction are primarily based on satellite NO_2 data in the warm season (May to September in the Northern Hemisphere) (Lu et al., 2015; Liu et al., 2016; Goldberg et al., 2021b). Lange et al. (2022) have proven that it is also possible to fit the NO_2 line densities for NO_x emissions and lifetimes in winter when NO_x lifetimes are much longer. Zhang et al. (2023) estimated a year-round daily NO_x emissions and lifetimes over Wuhan from September 2019 through August 2020. In this study, we extend the study period to 6 years. We have more than 40 valid days for each weekday and weekends, and more than 50 days for each season and each year (2018 excepted), making it possible to investigate the time variabilities of NO_x emissions over Wuhan on the weekly, seasonal, and interannual scales.

https://doi.org/10.5194/egusphere-2024-2641
Preprint. Discussion started: 18 September 2024

3.2.1 Weekly cycle

To identify the weekly cycle of NO_x emissions over Wuhan, we exclude the 25 valid days during the COVID-lockdown period, resulting in 310 valid daily NO_x emissions. The weekend effect (defined as the reduction in NO_2 columns or NO_x emissions on weekends compared to weekdays) is widely recognized and reported in cities around the world but not in Chinese cities (Beirle et al., 2003; Stavrakou et al., 2020; Zhang et al., 2023; Goldberg et al., 2021a). Beirle et al. (2003) explained the absence of a weekend effect in Chinese cities by the dominant role of power plants and industry in NO_x emission sources. Stavrakou et al. (2020) found a slight reduction of NO_2 columns on weekends compared to the weekday average in Chinese cities from 2005 to 2017. Because of China's clean air action on power plants and the growing vehicle population, transportation has replaced power plants as the dominant contributor to NO_x emissions. However, we still find no significant minimum on weekends, as shown in Figure 3. Cultural and living differences with other cities might explain the absence of a strong weekend effect in Wuhan. Shops, restaurants, and traffic are much busier on weekends, especially at noon when the satellite passes. We calculate an overall 0.95 weekend-to-weekday NO_x emission ratio, while Lange et al. (2022) reported the ratio of 0.79. We do not have a clear explanation for this difference. Actually, we find a NO_x emissions maximum on Thursday, which was also seen by Beirle et al. (2003) for Chinese cities. The weekday maximum is mostly seen on Fridays or Thursdays in cities in Europe and North America.

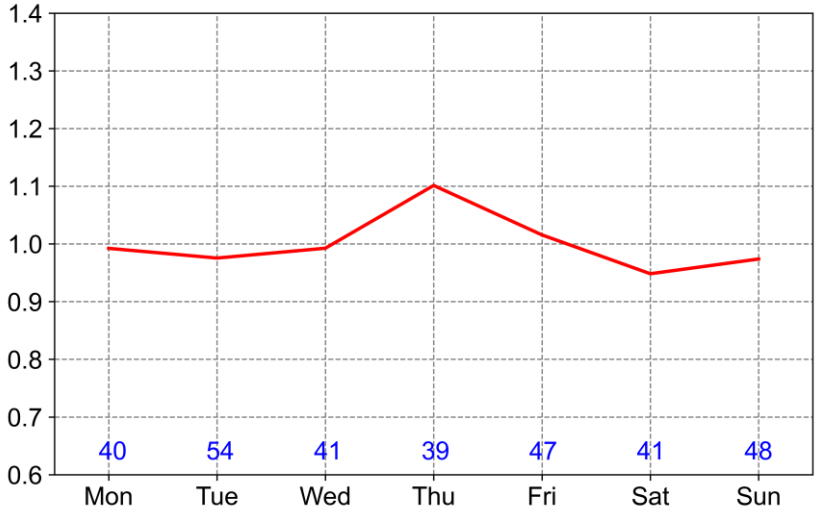

Figure 3: Weekly cycle of mean (2018—2023) NO_x emissions. The emissions are normalized with respect to the mean emissions of all the days. The number of days for each weekday and weekends is listed in the plot.

3.2.2 Seasonal pattern

Seasonal NO_x emissions over Wuhan are plotted in Figure 4a. Similar to the bottom-up emission inventories, our results reveal little variability in NO_x emissions between seasons. Winter emissions are slightly higher by 10.5%—14.5% than the

https://doi.org/10.5194/egusphere-2024-2641
Preprint. Discussion started: 18 September 2024

other three seasons. This is expected, for transportation and industry are the two dominant contributors to NO_x emissions over Wuhan, making up nearly 90% of the total NO_x emissions, and these two emission sectors exhibit no significant seasonal variations (Zheng et al., 2018). Also, Wuhan is located in central China where winter is mild, and there is no domestic heating in winter. The summer-to-winter NO_x emission ratio usually serves to indicate the relative importance of winter heating and summer power consumption due to air conditioning. Here we calculate a summer-to-winter ratio of 0.87, while Lange et al. (2022) reported 0.3. Their much lower summer-to-winter emission ratio may be caused by much lower estimated summertime NO_x emissions or much higher winter emissions or both.

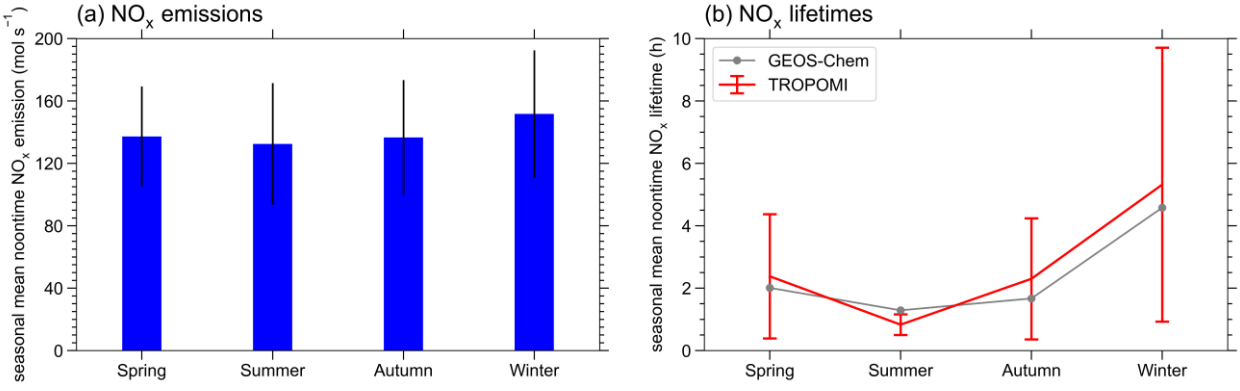

Figure 4: (a) TROPOMI estimated seasonal mean noontime NO_x emissions over Wuhan. (b) TROPOMI estimated (red line), and GEOS-Chem model produced (gray line) seasonal mean noontime NO_x lifetimes over Wuhan. The error bars represent the standard deviation.

Determined by the NO_x photochemical activity rate under the influence of temperature and OH concentrations, the NO_x lifetimes are longest in winter and shortest in summer, as shown in Figure 4b. Spring and autumn NO_x lifetimes are close to each other between winter and summer. A significant difference is seen in the summer lifetime estimation. Zhang et al. (2023) reported an average of 1.4 h, close to the GEOS-Chem model result (Figure 4b, gray line), and we calculate a lower 0.8 h, even lower than the 2—3 h calculated by Liu et al. (2016) for the warm season. We see much more substantial seasonal difference than Lange et al. (2022). We estimate an average of 5.3 h in winter lifetime and less than one h in summer, while the values are three h in winter and around 2 h for summer, as calculated by Lange et al. (2022). The GEOS-Chem results are between ours and those from Lange et al. (2022), with 4.6 h in winter and 1.3 h in summer. Our calculation is closer to the GEOS-Chem simulation, especially in winter. Given the observed satellite NO_2 line densities, the estimated NO_x emissions will be higher when the estimated lifetime is shorter, and the emissions lower otherwise. Therefore, we estimate higher summer NO_x emissions over Wuhan and lower winter emissions than Lange et al. (2022), leading to a much higher (also more realistic, considering the sectoral emission contributions) summer-to-winter emission ratio in this study. In this work, the a priori NO_x emissions are used to restrict the computation of NO_x emissions. Thereby, we have partly avoided the possible underestimation of NO_x emissions. This may also partly explain the much higher summer-to-winter NO_x

https://doi.org/10.5194/egusphere-2024-2641
Preprint. Discussion started: 18 September 2024

emission ratio in this work than in Lange et al. (2022), for they may have underestimated summer NO_x emissions over Wuhan.

3.2.3 Interannual variation

Stringent emission control strategies have been implemented in China to control NO_x emissions to combat air pollution since as early as 2010, and a nationwide NO_x emission reduction has been seen since 2012 (Zheng et al., 2018; Li et al., 2024a), and we find a similar trend over Wuhan from 2018 to 2023. Our calculation shows a slight increase (3.1%) in NO_x emissions over Wuhan from 2018 to 2019 (Figure 5). The outbreak of COVID-19 in early 2020 led to dramatic changes in NO_x emissions. Studies have investigated the reduction in satellite NO_2 columns (Bauwens et al., 2020) and NO_x emissions (e.g. Ding et al., 2020; Zheng et al., 2021; Lange et al., 2022) around the world due to the lockdown restrictions to combat the COVID-19. We have also found a more than 70% decrease in NO_x emissions over Wuhan in early February 2020 (Zhang et al., 2023). Although Wuhan reopened on 9 April 2020, we define the COVID-19 lockdown-influenced period as 23 January to the end of April, considering the slow recovery of human activities. There are 25 days with valid NO_x emissions estimation during this period, as shown in Figure 5. We calculated the lowest NO_x emissions of less than 20.0 mol s^{-1} during the lockdown, and the mean NO_x emissions in this period are 58% lower than the 2019 emission level. The mean emission during the other days in 2020 is comparable to 2019.

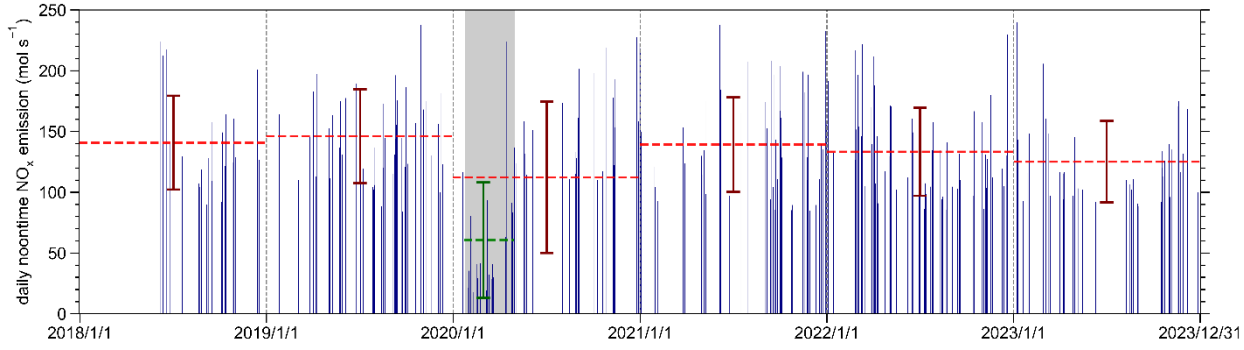

Figure 5: Daily NO_x noontime NO_x emissions over Wuhan on clear sky days from 13 May 2018 through 31 December 2023. The annual mean emissions for each year are marked as red dash lines, and the green dash line represents the mean NO_x emission during the COVID-19 lockdown-influenced period. The error bars denote the emission standard deviation for each time frame. The COVID-19 lockdown-influenced period is shaded in grey.

Overall, because of the COVID-19 lockdown, the 2020 annual mean emission is 23.6% below the 2019 level, while Lonsdale and Sun (2023) reported only 5% lower emissions over Wuhan in 2020 compared to 2019. NO_x emissions rebound by 21.6% from 2020 to 2021 but are still 7.2% less than the 2019 level. In 2022, we find 9.6% lower NO_x emissions below 2019, while Lonsdale and Sun (2023) reported a larger 26%. A further 6.7% NO_x emission reduction over Wuhan is seen in 2023 under 2022.

https://doi.org/10.5194/egusphere-2024-2641
Preprint. Discussion started: 18 September 2024

3.3 Wind field dependence of emission and lifetime estimations

Ideally, NO_x emissions and chemical loss rate directly derived from the satellite observations in combination with the wind fields should be insensitive to the wind direction and even wind speed. However, Valin et al. (2013) showed that the chemical NO_x lifetime in a city plume is wind speed dependent and shorter under strong winds. This suggests that it is inappropriate to average the NO_2 plumes at all wind speeds to obtain the mean OH concentration. In our study, we treat every plume separately to estimate the removal rate of NO_x over the city, and this provides us with the opportunity to investigate the dependence of estimated NO_x lifetimes and emissions on the wind direction and speed.

3.3.1 Wind direction

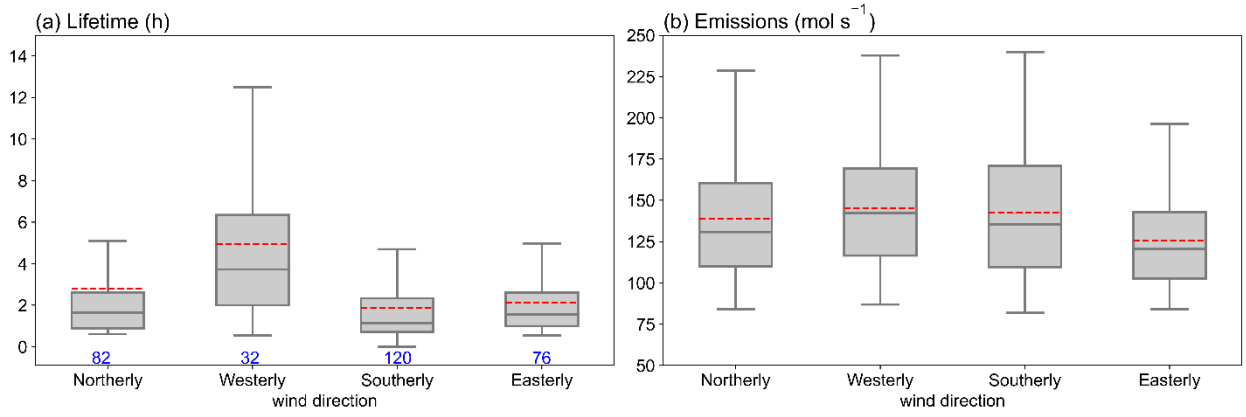

Figure 6: Boxplots of estimated NO_x (a) lifetimes and (b) emissions over Wuhan are categorized into four groups based on wind direction. For each box, the middle line indicates the median; the box top and bottom indicate the upper and lower quartiles, respectively; the whiskers indicate the farthest nonoutlier values; and the means are presented with red dashed lines. The number of days in each category is listed in blue.

We separate the 310 valid calculations by wind direction (northerly wind: 315°—45°, westerly wind: 225°—315°, southerly wind: 135°—225°, and easterly wind: 45°—135°) and compare the estimated NO_x lifetimes and emissions in each category in Figure 6. The variation in NO_x lifetimes with wind direction is closely related to the seasonal prevailing wind direction. About 1/3 of the winter winds are from the west; consequently, we compute the longest NO_x lifetimes under westerly winds. On the contrary, summer is dominated by southerly wind, resulting in the shortest NO_x lifetime under this wind direction. We have found in Section 3.2 that the seasonal variation in NO_x emissions is slight in Wuhan. Hence, the dependence of NO_x emission estimation on wind direction is not likely influenced much by the season. We find that NO_x emissions vary little with wind directions, except that estimated NO_x emissions under the easterly wind condition are ~10% lower than the 310 days mean. When looking at tropospheric NO_2 columns over Wuhan (Figure 1b), we find that it is relatively clean to the north, west, and south of Wuhan, but there are high NO_2 spots to the east of the city. Although we

https://doi.org/10.5194/egusphere-2024-2641
Preprint. Discussion started: 18 September 2024

have tried to avoid the influence of upwind emissions by assuming a linear change in the background NO_2 columns (Zhang et al., 2023), the finding here indicates that it is insufficient. The high NO_2 columns at the starting point of the NO_2 line density will lead to underestimating city NO_x emissions; the days with distinct upwind NO_x emissions should be treated cautiously in future calculations.

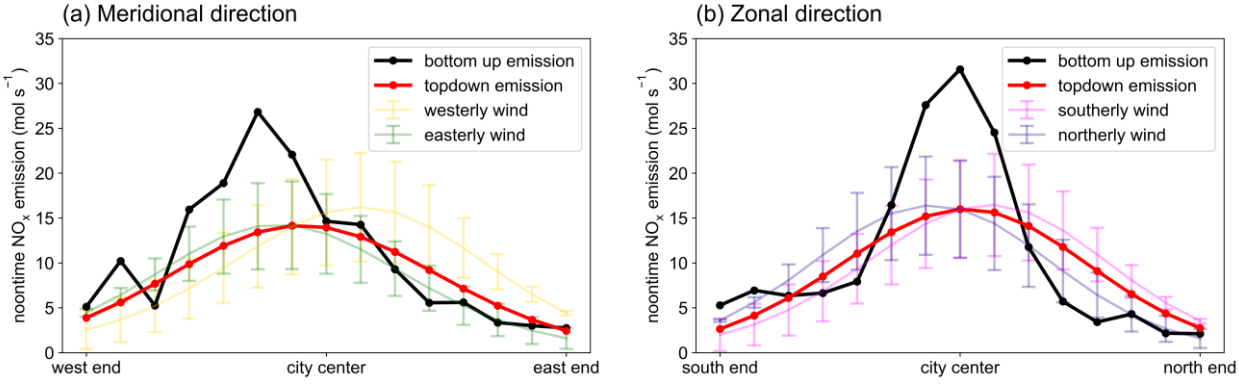

Figure 7: Fitted emission distribution in the (a) meridional direction and (b) zonal direction, the bottom-up emission distribution in the corresponding direction is plotted in a black line.

The fitted emission distribution under each wind direction is also compared in Figure 7. We can see clear mirrored distributions between the westerly and easterly wind direction (Figure 7a) and the southerly and northerly wind direction (Figure 7b). This can be explained by the fact that the windy conditions disperse quickly NO_2 away to the downwind region (Goldberg et al., 2024). Finally, the fitted emission distribution in the zonal and meridional directions are basically in line with those from the bottom-up emission inventory, with the difference that the fitted emission distributions are flatter.

3.3.2 Wind speed

We then sort our 310 days with valid NO_x emission calculations into four categories according to wind speed: slow wind (0–3 m s^{-1}), medium slow wind (3–5 m s^{-1}), medium fast wind (5–7 m s^{-1}), and fast wind (> 7 m s^{-1}). We have more than 27 valid calculations for each category, and the corresponding lifetime and NO_x emissions are shown in Figure 8. We find that NO_x lifetimes change little when wind speed is less than 7 m s^{-1}, varying from 2.4 h (5–7 m s^{-1}) to 2.6 h (0–3 m s^{-1}). However, a 32% shorter NO_x lifetime at fast wind speed (> 7 m s^{-1}) is seen compared to the slow wind speed (< 5 m s^{-1}), in accordance with the 31% difference calculated by Valin et al. (2013).

https://doi.org/10.5194/egusphere-2024-2641
Preprint. Discussion started: 18 September 2024

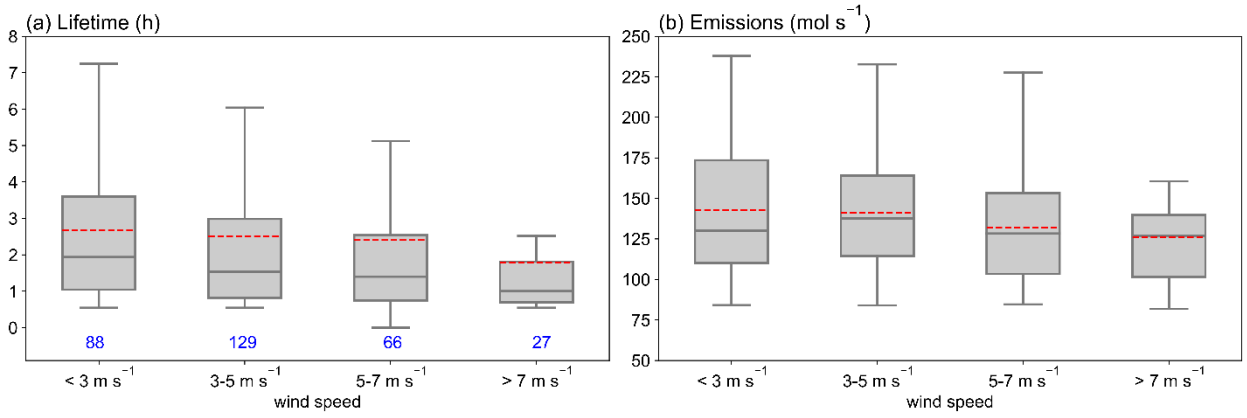

Figure 8: Same as Figure 6 but with the wind speed.

Surprisingly, we also estimate slightly lower (about 9%) NO_x emissions when wind speed is fast. It may be explained that the fast wind speed leads to strong ventilation of NO_2 and, thus, lower estimated NO_x emissions. It has a small influence (less than 1% in Wuhan's case) on the overall estimation of city NO_x emissions, for the days with fast wind make up only less than 10% of the total number of days. The low bias should be considered for cities with a large proportion of fast winds.

3.3.3 Uncertainties

The uncertainties of NO_x emissions and lifetimes estimation come from the parameters and quantities used during the fitting procedure. The primary sources of uncertainties include:

—The systematic error in TROPOMI NO_2 data. The TROPOMI version 2.4.0—2.6.0 data made significant improvements from the earlier versions, and there is a ~20% difference compared to the ground-based data at the Xianghe site in North China (Keppens and Lambert, 2023); we have corrected the possible underestimation over Wuhan by a factor of 1.2, but we thus we still conservatively consider a 20% uncertainty in the NO_2 column.

—The bias in the a priori OH concentration. In our previous work (Zhang et al., 2023), we limited the OH concentration between the 0.8—1.2 interval of GEOS-Chem simulated OH concentration and found that the estimated OH concentration in more than 90% of the days fell in this interval, so we exerted a 20% uncertainty on OH concentration. In this study, we conservatively choose the uncertainty of 30% following Lange et al. (2022).

—Influence of upwind emissions. Previous work using the superposition column model (Lorente et al., 2019; Zhang et al., 2023) did not consider the influence of NO_x emissions in the surrounding area on the estimation of city NO_x emissions. In this work, we find a 10% anomaly in estimated NO_x emission for Wuhan when there are distinct hotspots of NO_2 in the upwind region. We thus take the 10% uncertainty to represent the influence of upwind emissions. We must clarify that this part of the uncertainty is 'city-specific.' It can be neglected for some isolated cities or large point sources like Paris or

https://doi.org/10.5194/egusphere-2024-2641
Preprint. Discussion started: 18 September 2024

Riyadh. For other cities located in polluted backgrounds, the uncertainty introduced by upwind emissions should be calculated accordingly, and it is not necessarily to be 10%.

—Bottom-up NO_x emissions, the NO_x/NO_2 ratio, and the wind fields. Uncertainty in bottom-up emission inventory is 35%, as stated in Sect. 2.3. Uncertainty arising from NO_x/NO_2 ratio and the wind field are 10% and 20%, respectively, in accordance with those from Zhang et al. (2023).

Finally, we use the root-mean-square sum of all the above contributions, resulting in a 54% uncertainty for the NO_x emissions and lifetimes estimated for Wuhan.

To be mentioned, Zhang et al. (2023) also considered the uncertainty caused by the area of the study domain, and they found a 15% uncertainty caused by the domain size. In this study, we leave out the consideration of this part of the uncertainty source because our study domain is limited to the urban area of Wuhan, and it is a proper size to estimate NO_x emissions in the urban area.

4 Conclusion

In this work, we use the superposition column model to calculate city NO_x emissions and lifetimes on a daily basis, with a time span of nearly six years, from May 2018 to December 2023. The city of Wuhan is used as an example to investigate the seasonal pattern, weekly cycle, and interannual variation of city NO_x emissions. The dependence of estimated NO_x emissions and lifetimes on the wind direction and speed are also discussed. We chose the urban area of Wuhan as our study domain, about 90 km in diameter. For each clear sky day with a homogeneous wind field, we sample the TROPOMI NO_2 column data in the grid size of 6 km × 6 km and rotate it with the wind direction. Then, every 15 grid cells perpendicular to the wind direction are accumulated to form the NO_2 line density. The NO_2 line density is fitted with the superposition column model to obtain the final daily NO_x emissions and lifetimes.

For the period from May 2018 to December 2023, we obtain 335 days with valid NO_x emissions and lifetimes estimations over Wuhan, with more than 50 days for each season and each year (2018 excepted) and more than 40 days for each weekday and weekends. The monthly NO_x emissions for the years 2018 and 2019 are compared with those from EDGAR and ABACAS bottom-up emission inventories, respectively. We see 39% lower NO_x emissions over Wuhan compared to the EDGAR v6.1 dataset, and the difference is only 4.7% compared to the ABACAS inventory. We find a moderate seasonal variation with a relatively high (0.87) summer-to-winter NO_x emission ratio. This can partly be explained by the fact that we use the ABACAS bottom-up NO_x emissions as one of the limiting factors to constrain the top-down emissions, avoiding the possible underestimation of NO_x emissions in the summertime when NO_2 columns are rather low. The estimated noontime NO_x lifetimes vary from less than 1 h in summer to 5.3 h in winter, with an average of 2.6 h. We see only a slight drop in NO_x emissions on weekends (the weekend-to-weekday ratio is 0.95) over Wuhan, which may relate to the living culture and style of the Chinese. We find that NO_x emissions over Wuhan during the COVID-19 lockdown-influenced period are nearly

https://doi.org/10.5194/egusphere-2024-2641
Preprint. Discussion started: 18 September 2024

60% lower than the normal level and rebound to the 2019 emission level for the rest of 2020. Overall, our calculations reveal a steady decline in NO_x emissions from 2019 to 2023, and the emissions in 2023 are 15.6% below the 2019 level.

We separate the 310 days (25 days during the COVID-19 lockdown excluded) of NO_x emissions and lifetimes according to wind direction and speed. We find a ~10% lower estimated NO_x emissions in the condition with distinct upwind emissions, indicating that we need to be more careful in the future when computing NO_x emissions over cities or large point sources located in a polluted background. We also see 30% shorter NO_x lifetime under fast wind.

We have demonstrated in this work by combining the superposition column model and the high spatial resolution TROPOMI NO_2 column product one can investigate the variability of NO_x emissions and lifetimes on daily to annual time scale. We also provide recommendations for dealing with conditions with upwind emissions for better and more accurate city NO_x emissions estimations. So far, the superposition column model has only been used for two cities, Paris and Wuhan; we will extend it to other cities and emission sources in the future.

Author contributions. QZ and KFB designed the research. QZ did the processing, visualizations and main writing. KFB edited the paper. CL and AM provided improvements in the method. BZ and SL provided the ABACAS emission inventory. YP reviewed the paper.

Competing interests. The authors declare no competing financial interest.

Acknowledgement. This work is supported by the National Natural Science Foundation of China (grant no. 42375106 and 41805098) and the National Key R&D Program of China (No. 2023YFB3907500). The Copernicus Sentinel-5P level-2 NO_2 data are employed in this work. Sentinel-5 Precursor is a European Space Agency (ESA) mission on behalf of the European Commission (EC). The TROPOMI payload is a joint development by ESA and the Netherlands Space Office. The Sentinel-5 Precursor ground segment development has been funded by ESA and with national contributions from the Netherlands, Germany, and Belgium. The Wind fields used in this study are provided by ECMWF ERA5. EDGAR v6.1 Global Air Pollutant Emissions are provided by https://edgar.jrc.ec.europa.eu/dataset_ap61 (last access: 13 September 2024).

Data availability. The TROPOMI NO_2 data can be freely downloaded from the Tropospheric Emission Monitoring Internet Service (https://www.temis.nl/airpollution/no2.php). The ERA5 data can be found at the Copernicus Climate Change (C3S) climate data store (CDS) (https://cds.climate.copernicus.eu/cdsapp#!/dataset/reanalysis-era5-pressure-levels?tab=overview).

References

Baklanov, A., Molina, L. T., and Gauss, M.: Megacities, air quality and climate, Atmospheric Environment, 126, 235-249, 10.1016/j.atmosenv.2015.11.059, 2016.

https://doi.org/10.5194/egusphere-2024-2641
Preprint. Discussion started: 18 September 2024

Bauwens, M., Compernolle, S., Stavrakou, T., Muller, J. F., van Gent, J., Eskes, H., Levelt, P. F., van der, A. R., Veefkind, J. P., Vlietinck, J., Yu, H., and Zehner, C.: Impact of coronavirus outbreak on NO_2 pollution assessed using TROPOMI and OMI observations, Geophysical Research Letters, 47, e2020GL087978, 10.1029/2020GL087978, 2020.
Beirle, S., Platt, U., Wenig, M., and Wagner, T.: Weekly cycle of NO_2 by GOME measurements: a signature of anthropogenic sources, Atmospheric Chemistry and Physics, 3, 2225-2232, doi: 10.5194/acp-3-2225-2003, 2003.
Beirle, S., Boersma, K. F., Platt, U., Lawrence, M. G., and Wagner, T.: Megacity emissions and lifetimes of nitrogen oxides probed from space, Science, 333, 1737-1739, 10.1126/science.1207824, 2011.
Beirle, S., Borger, C., Dorner, S., Li, A., Hu, Z., Liu, F., Wang, Y., and Wagner, T.: Pinpointing nitrogen oxide emissions from space, Science Advances, 5, eaax9800, doi: 10.1126/sciadv.aax9800, 2019.
Bovensmann, H., Burrows, J. P., Buchwitz, M., Frerick, J., Noel, S., Rozanov, V., Chance, K., and Goede, A.: SCIAMACHY: Mission Objectives and Measurement Modes, Journal of the Atmospheric Sciences, 56, 127-150, 1999.
Burrows, J. P., Weber, M., Buchwitz, M., Rozanov, V., Ladstatter-Weibenmayer, A., Richter, A., DeBeek, R., Hoogen, R., Bramstedt, K., Eichmann, K.-U., Eisinger, M., and Perner, D.: The Global Ozone Monitoring Experiment (GOME): Mission Concept and First Scientific Results, Journal of the Atmospheric Sciences, 56, 151-175, https://doi.org/10.1175/1520-0469(1999)056<0151:TGOMEG>2.0.CO;2, 1999.
Butler, T. M., Lawrence, M. G., Gurjar, B. R., van Aardenne, J., Schultz, M., and Lelieveld, J.: The representation of emissions from megacities in global emission inventories, Atmospheric Environment, 42, 703-719, 10.1016/j.atmosenv.2007.09.060, 2008.
de Foy, B., Lu, Z., Streets, D. G., Lamsal, L. N., and Duncan, B. N.: Estimates of power plant NO_x emissions and lifetimes from OMI NO_2 satellite retrievals, Atmospheric Environment, 116, 1-11, 10.1016/j.atmosenv.2015.05.056, 2015.
de Foy, B., Wilkins, J. L., Lu, Z., Streets, D. G., and Duncan, B. N.: Model evaluation of methods for estimating surface emissions and chemical lifetimes from satellite data, Atmospheric Environment, 98, 66-77, 10.1016/j.atmosenv.2014.08.051, 2014.
Ding, J., van der A, R. J., Mijling, B., and Levelt, P. F.: Space-based NO_x emission estimates over remote regions improved in DECSO, Atmospheric Measurement Techniques, 10, 925-938, 10.5194/amt-10-925-2017, 2017.
Ding, J., van der A, R. J., Eskes, H. J., Mijling, B., Stavrakou, T., Geffen, J. H. G. M., and Veefkind, J. P.: NO_x Emissions Reduction and Rebound in China Due to the COVID-19 Crisis, Geophysical Research Letters, 47, e2020GL089912, 10.1029/2020gl089912, 2020.
Eskes, H., Eichmann, K.-U., Lambert, J.-C., Loyola, D. G., Stein-Zweers, D., Dehn, A., and Zehner, C.: S5P MPC Product Readme Nitrogen Dioxide, https://doi.org/10.5270/S5P-9bnp8q8, 2023.
Geng, G., Zhang, Q., Tong, D., Li, M., Zheng, Y., Wang, S., and He, K.: Chemical composition of ambient $PM_{2.5}$ over China and relationship to precursor emissions during 2005–2012, Atmospheric Chemistry and Physics, 17, 9187-9203, 10.5194/acp-17-9187-2017, 2017.
Goldberg, D. L., Anenberg, S. C., Kerr, G. H., Mohegh, A., Lu, Z., and Streets, D. G.: TROPOMI NO_2 in the United States: A Detailed Look at the Annual Averages, Weekly Cycles, Effects of Temperature, and Correlation With Surface NO_2 Concentrations, Earth's Future, 9, e2020EF001665, doi: 10.1029/2020EF001665, 2021a.
Goldberg, D. L., Anenberg, S. C., Lu, Z., Streets, D. G., Lamsal, L. N., McDuffie, E. E., and Smith, S. J.: Urban NO_x emissions around the world declined faster than anticipated between 2005 and 2019, Environmental Research Lettters, 16, 115004, doi: 10.1088/1748-9326/ac2c34, 2021b.
Goldberg, D. L., Lu, Z., Streets, D. G., De Foy, B., Griffin, D., Mclinden, C. A., Lamsal, L. N., Krotkov, N. A., and Eskes, H.: Enhanced capabilities of TROPOMI NO_2: estimating NO_x from North American cities and power plants, Environmental Science & Technology, 53, 12594-12601, 10.1021/acs.est.9b04488, 2019.
Goldberg, D. L., Tao, M., Kerr, G. H., Ma, S., Tong, D. Q., Fiore, A. M., Dickens, A. F., Adelman, Z. E., and Anenberg, S. C.: Evaluating the spatial patterns of U.S. urban NOx emissions using TROPOMI NO_2, Remote Sensing of Environment, 300, 10.1016/j.rse.2023.113917, 2024.
Hersbach, H., Bell, B., Berrisford, P., Hirahara, S., Horányi, A., Muñoz-Sabater, J., Nicolas, J., Peubey, C., Radu, R., Schepers, D., Simmons, A., Soci, C., Abdalla, S., Abellan, X., Balsamo, G., Bechtold, P., Biavati, G., Bidlot, J., Bonavita, M., Chiara, G., Dahlgren, P., Dee, D., Diamantakis, M., Dragani, R., Flemming, J., Forbes, R., Fuentes, M., Geer, A., Haimberger, L., Healy, S., Hogan, R. J., Hólm, E., Janisková, M., Keeley, S., Laloyaux, P., Lopez, P., Lupu, C., Radnoti, G., Rosnay, P., Rozum, I., Vamborg, F., Villaume, S., and Thépaut, J. N.: The ERA5 global reanalysis, Quarterly Journal of the Royal Meteorological Society, 146, 1999-2049, 10.1002/qj.3803, 2020.
Jacob, D.: Introduction to Atmospheric Chemistry, Princeton Univ. Press, 1999.
Keppens, A. and Lambert, J.-C.: Quarterly Validation Report of the Copernicus Sentinel-5 Precursor Operational Data Products #21: April 2018 - November 2023, https://mpc-vdaf.tropomi.eu, 2023.
Kharol, S. K., Martin, R. V., Philip, S., Boys, B., Lamsal, L. N., Jerrett, M., Brauer, M., Crouse, D. L., McLinden, C., and Burnett, R. T.: Assessment of the magnitude and recent trends in satellite-derived ground-level nitrogen dioxide over North America, Atmospheric Environment, 118, 236-245, 10.1016/j.atmosenv.2015.08.011, 2015.
Kong, H., Lin, J., Zhang, R., Liu, M., Weng, H., Ni, R., Chen, L., Wang, J., Yan, Y., and Zhang, Q.: High-resolution ($0.05° \times 0.05°$) NO_x emissions in the Yangtze River Delta inferred from OMI, Atmospheric Chemistry and Physics, 19, 12835-12856, 10.5194/acp-19-12835-2019, 2019.

https://doi.org/10.5194/egusphere-2024-2641
Preprint. Discussion started: 18 September 2024

Lamsal, L. N., Martin, R. V., Padmanabhan, A., van Donkelaar, A., Zhang, Q., Sioris, C. E., Chance, K., Kurosu, T. P., and Newchurch, M. J.: Application of satellite observations for timely updates to global anthropogenic NO_x emission inventories, Geophysical Research Letters, 38, L05810, doi: 10.1029/2010gl046476, 2011.

Lange, K., Richter, A., and Burrows, J. P.: Variability of nitrogen oxide emission fluxes and lifetimes estimated from Sentinel-5P TROPOMI observations, Atmospheric Chemistry and Physics, 22, 2745-2767, doi: 10.5194/acp-22-2745-2022, 2022.

Levelt, P. F., van den Oord, G. H. J., Dobber, M. R., Malkki, A., Huib, V., Johan de, V., Stammes, P., Lundell, J. O. V., and Saari, H.: The ozone monitoring instrument, IEEE Transactions on Geoscience and Remote Sensing, 44, 1093-1101, doi: 10.1109/tgrs.2006.872333, 2006.

Li, H., Zheng, B., Lei, Y., Hauglustaine, D., Chen, C., Lin, X., Zhang, Y., Zhang, Q., and He, K.: Trends and drivers of anthropogenic NO emissions in China since 2020, Environmental Science and Ecotechnology, 21, 10.1016/j.ese.2024.100425, 2024a.

Li, K., Jacob, D. J., Liao, H., Zhu, J., Shah, V., Shen, L., Bates, K. H., Zhang, Q., and Zhai, S.: A two-pollutant strategy for improving ozone and particulate air quality in China, Nature Geoscience, 12, 906-910, 10.1038/s41561-019-0464-x, 2019.

Li, M., Kurokawa, J., Zhang, Q., Woo, J.-H., Morikawa, T., Chatani, S., Lu, Z., Song, Y., Geng, G., Hu, H., Kim, J., Cooper, O. R., and McDonald, B. C.: MIXv2: a long-term mosaic emission inventory for Asia (2010–2017), Atmospheric Chemistry and Physics, 24, 3925-3952, doi: 10.5194/acp-24-3925-2024, 2024b.

Liu, F., Beirle, S., Zhang, Q., Dörner, S., He, K., and Wagner, T.: NO_x lifetimes and emissions of cities and power plants in polluted background estimated by satellite observations, Atmospheric Chemistry and Physics, 16, 5283-5298, 10.5194/acp-16-5283-2016, 2016.

Liu, F., Tao, Z., Beirle, S., Joiner, J., Yoshida, Y., Smith, S. J., Knowland, K. E., and Wagner, T.: A new method for inferring city emissions and lifetimes of nitrogen oxides from high-resolution nitrogen dioxide observations: a model study, Atmospheric Chemistry and Physics, 22, 1333-1349, 10.5194/acp-22-1333-2022, 2022.

Lonsdale, C. R. and Sun, K.: Nitrogen oxides emissions from selected cities in North America, Europe, and East Asia observed by the TROPOspheric Monitoring Instrument (TROPOMI) before and after the COVID-19 pandemic, Atmospheric Chemistry and Physics, 23, 8727-8748, 10.5194/acp-23-8727-2023, 2023.

Lorente, A., Boersma, K. F., Eskes, H. J., Veefkind, J. P., van Geffen, J., de Zeeuw, M. B., Denier van der Gon, H. A. C., Beirle, S., and Krol, M. C.: Quantification of nitrogen oxides emissions from build-up of pollution over Paris with TROPOMI, Scitific Report, 9, 20033, doi: 10.1038/s41598-019-56428-5, 2019.

Lu, X., Zhang, L., Chen, Y., Zhou, M., Zheng, B., Li, K., Liu, Y., Lin, J., Fu, T.-M., and Zhang, Q.: Exploring 2016–2017 surface ozone pollution over China: source contributions and meteorological influences, Atmospheric Chemistry and Physics, 19, 8339-8361, 10.5194/acp-19-8339-2019, 2019.

Lu, Z., Streets, D. G., de Foy, B., Lamsal, L. N., Duncan, B. N., and Xing, J.: Emissions of nitrogen oxides from US urban areas: estimation from Ozone Monitoring Instrument retrievals for 2005-2014, Atmospheric Chemistry and Physics, 15, 10367-10383, doi: 10.5194/acp-15-10367-2015, 2015.

Martin, R. V.: Global inventory of nitrogen oxide emissions constrained by space-based observations of NO_2 columns, Journal of Geophysical Research, 108, doi: 10.1029/2003jd003453, 2003.

Park, H., Jeong, S., Park, H., Labzovskii, L. D., and Bowman, K. W.: An assessment of emission characteristics of Northern Hemisphere cities using spaceborne observations of CO_2, CO, and NO_2, Remote Sensing of Environment, 254, 10.1016/j.rse.2020.112246, 2021.

Rey-Pommier, A., Chevallier, F., Ciais, P., Broquet, G., Christoudias, T., Kushta, J., Hauglustaine, D., and Sciare, J.: Quantifying NO_x emissions in Egypt using TROPOMI observations, Atmospheric Chemistry and Physics, 22, 11505-11527, 10.5194/acp-22-11505-2022, 2022.

Stavrakou, T., Muller, J. F., Bauwens, M., Boersma, K. F., and van Geffen, J.: Satellite evidence for changes in the NO_2 weekly cycle over large cities, Scientific Report, 10, 10066, doi: 10.1038/s41598-020-66891-0, 2020.

Valin, L. C., Russell, A. R., and Cohen, R. C.: Variations of OH radical in an urban plume inferred from NO_2 column measurements, Geophysical Research Letters, 40, 1856-1860, 10.1002/grl.50267, 2013.

van Geffen, J., Boersma, K. F., Eskes, H., Sneep, M., ter Linden, M., Zara, M., and Veefkind, J. P.: S5P TROPOMI NO_2 slant column retrieval: method, stability, uncertainties and comparisons with OMI, Atmospheric Measurement Techniques, 13, 1315-1335, 10.5194/amt-13-1315-2020, 2020.

van Geffen, J., Eskes, H., Compernolle, S., Pinardi, G., Verhoelst, T., Lambert, J.-C., Sneep, M., ter Linden, M., Ludewig, A., Boersma, K. F., and Veefkind, J. P.: Sentinel-5P TROPOMI NO_2 retrieval: impact of version v2.2 improvements and comparisons with OMI and ground-based data, Atmospheric Measurement Techniques, 15, 2037-2060, 10.5194/amt-15-2037-2022, 2022.

Veefkind, J. P., Aben, I., McMullan, K., Förster, H., de Vries, J., Otter, G., Claas, J., Eskes, H. J., de Haan, J. F., Kleipool, Q., van Weele, M., Hasekamp, O., Hoogeveen, R., Landgraf, J., Snel, R., Tol, P., Ingmann, P., Voors, R., Kruizinga, B., Vink, R., Visser, H., and Levelt, P. F.: TROPOMI on the ESA Sentinel-5 Precursor: A GMES mission for global observations of the atmospheric composition for climate, air quality and ozone layer applications, Remote Sensing of Environment, 120, 70-83, 10.1016/j.rse.2011.09.027, 2012.

Visser, A. J., Boersma, K. F., Ganzeveld, L. N., and Krol, M. C.: European NO_x emissions in WRF-Chem derived from OMI: impacts on summertime surface ozone, Atmospheric Chemistry and Physics, 19, 11821-11841, 10.5194/acp-19-11821-2019, 2019.

https://doi.org/10.5194/egusphere-2024-2641
Preprint. Discussion started: 18 September 2024

Xing, J., Li, S. M., Zheng, S., Liu, C., Wang, X., Huang, L., Song, G., He, Y., Wang, S., Sahu, S. K., Zhang, J., Bian, J., Zhu, Y., Liu, T.-Y., and Hao, J.: Rapid Inference of nitrogen oxide emissions based on a top-down method with a physically informed variational autoencoder, Environmental Science & Technology, 56, 12, 10.1021/acs.est.1c08337, 2022.

Zhai, S., Jacob, D. J., Wang, X., Liu, Z., Wen, T., Shah, V., Li, K., Moch, J. M., Bates, K. H., Song, S., Shen, L., Zhang, Y., Luo, G., Yu, F., Sun, Y., Wang, L., Qi, M., Tao, J., Gui, K., Xu, H., Zhang, Q., Zhao, T., Wang, Y., Lee, H. C., Choi, H., and Liao, H.: Control of particulate nitrate air pollution in China, Nature Geoscience, 14, 389-395, 10.1038/s41561-021-00726-z, 2021.

Zhang, L., Liu, L., Zhao, Y., Gong, S., Zhang, X., Henze, D. K., Capps, S. L., Fu, T.-M., Zhang, Q., and Wang, Y.: Source attribution of particulate matter pollution over North China with the adjoint method, Environmental Research Letters, 10, 10.1088/1748-9326/10/8/084011, 2015.

Zhang, Q., Boersma, K. F., Zhao, B., Eskes, H., Chen, C., Zheng, H., and Zhang, X.: Quantifying daily NO_x and CO_2 emissions from Wuhan using satellite observations from TROPOMI and OCO-2, Atmospheric Chemistry and Physics, 23, 551-563, doi: 10.5194/acp-23-551-2023, 2023.

Zhang, Q., Pan, Y., He, Y., Walters, W. W., Ni, Q., Liu, X., Xu, G., Shao, J., and Jiang, C.: Substantial nitrogen oxides emission reduction from China due to COVID-19 and its impact on surface ozone and aerosol pollution, Science of The Total Environment, 753, 142238, 10.1016/j.scitotenv.2020.142238, 2021.

Zhao, B., Wang, S. X., Liu, H., Xu, J. Y., Fu, K., Klimont, Z., Hao, J. M., He, K. B., Cofala, J., and Amann, M.: NO_x emissions in China: historical trends and future perspectives, Atmospheric Chemistry and Physics, 13, 9869-9897, 10.5194/acp-13-9869-2013, 2013.

Zhao, B., Zheng, H., Wang, S., Smith, K. R., Lu, X., Aunan, K., Gu, Y., Wang, Y., Ding, D., Xing, J., Fu, X., Yang, X., Liou, K. N., and Hao, J.: Change in household fuels dominates the decrease in $PM_{2.5}$ exposure and premature mortality in China in 2005-2015, Proceedings of the National Academy of Sciences, 115, 12401-12406, 10.1073/pnas.1812955115, 2018.

Zheng, B., Zhang, Q., Geng, G., Chen, C., Shi, Q., Cui, M., Lei, Y., and He, K.: Changes in China's anthropogenic emissions and air quality during the COVID-19 pandemic in 2020, Earth System Science Data, 13, 2895-2907, 10.5194/essd-13-2895-2021, 2021.

Zheng, B., Tong, D., Li, M., Liu, F., Hong, C., Geng, G., Li, H., Li, X., Peng, L., Qi, J., Yan, L., Zhang, Y., Zhao, H., Zheng, Y., He, K., and Zhang, Q.: Trends in China's anthropogenic emissions since 2010 as the consequence of clean air actions, Atmospheric Chemistry and Physics, 18, 14095-14111, doi: 10.5194/acp-18-14095-2018, 2018.

Zheng, H., Zhao, B., Wang, S., Wang, T., Ding, D., Chang, X., Liu, K., Xing, J., Dong, Z., Aunan, K., Liu, T., Wu, X., Zhang, S., and Wu, Y.: Transition in source contributions of $PM_{2.5}$ exposure and associated premature mortality in China during 2005-2015, Environment International, 132, 105111, 10.1016/j.envint.2019.105111, 2019.